Novel Theranostic DNA Nanoscaffolds for the Simultaneous Detection and Killing of *Escherichia coli* and *Staphylococcus aureus*

Magdiel I. Setyawati,[†,‡] Rajaletchumy Veloo Kutty,[†,‡] Chor Yong Tay,[‡] Xun Yuan,[‡] Jianping Xie,*[,‡] and David T. Leong*[,‡,§]

[‡]Department of Chemical and Biomolecular Engineering, National University of Singapore, 4 Engineering 4, Singapore 117585, Singapore

[§]NUS Graduate School for Integrative Science and Engineering, National University of Singapore, 28 Medical Drive, Singapore 117456, Singapore

Ⓢ *Supporting Information*

ABSTRACT: A novel theranostic platform is made by utilizing a self-assembled DNA nanopyramid (DP) as scaffold for incorporation of both detection and therapeutic moieties to combat bacterial infection. Red-emissive glutathione-protected gold nanoclusters (GSH-Au NCs) were used for bacterial detection. Actinomycin D (AMD) that was intercalated on the DP scaffold was used as therapeutic agent. This results in the formation of theranostic DPAu/AMD. Model bacteria *Escherichia coli* and *Staphylococcus aureus* were found to be readily taken in the DPAu/AMD and be susceptible to its killing effect. In addition, DPAu/AMD was observed to outperform the free AMD in killing infectious bacteria. The degradation of the DP structure by DNase was found to be responsible for the release of AMD and the effective killing effect of the infectious bacteria. This novel strategy presents a basic platform for future improvements to detect infectious bacteria and treatment.

KEYWORDS: *theranostic, DNA nanopyramid, infection, antibacterial, actinomycin D, gold nanoclusters*
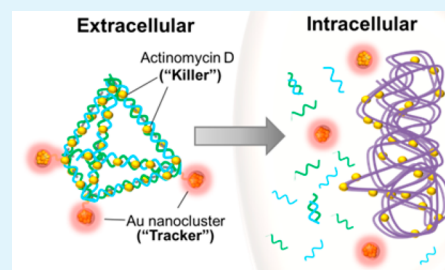
INTRODUCTION

Infectious microorganisms could lay latent in humans.[1] This poses a problem in treating infection, as most antimicrobial drugs have difficulty crossing the mammalian barriers.[2] Nanomedicine offers one of the promising strategies to overcome this infection problem. The nanocarrier preserves the antimicrobial compound activity by protecting it against chemical and enzyme degradations[3,4] until it reaches the target bacteria. In addition, nanomedicine allows a more engineered transport across the cell membrane. These nanocarriers have been crafted from various types of materials, such as polymers, lipids, metals and metal oxides.[1,2,5−10] Nevertheless, these materials are not without limitation. Polymers and lipids are usually heterogeneous in nature, making them unsuitable for higher ordered structures.[5] In contrast, inorganic nanomaterials could be easily controlled to give the desired delivery properties. However, recent studies show that inorganic-based nanomaterials can induce toxicity, dysfunction, and anomaly to the mammalian cell system.[11−17] Hence there is a need to look for alternative materials that could accomplish the original task of delivering antimicrobial agents without eliciting ill effects to the patients' healthy cells. DNA nanostructures are the new emerging materials for nanomedicine with application ranging from delivery carriers and diagnostics.[5,18−20] Making use of nucleic base complementary pairing, one could design nanostructures with any desired size and configuration with precise control. To date, planar sheets, tubes, tetrahedral, bipyramids, cubes, cages, and other previously unheard of 3D DNA structures could be realized with double stranded DNA (dsDNA) as their base material.[5,19−23] In addition, proteins, ligands, oligonucleotides, or other small functional compounds with bioimaging moieties could be site-specifically attached onto these DNA nanostructures, adding further to the base nanostructure repertoire.[5,22,23] Surfaces of planar DNA could be functionalized with protein or nanoparticles, resulting in the formation of grids for diagnostic purpose.[23−25] Commercial strand modifiers (e.g., −thiol end modifier) allow the conjugation of different sizes of gold nanoparticles in site specific manner to the DNA strands.[26] DNA backbone modification and nucleotide replacement approaches could be used as an alternative route to achieve site specific modification of the DNA nanostructures.[23] The high precision coupled with the fact that DNA is inherently nontoxic to cells[18] allows us to tailor a useful platform to both visualize and combat microbial infection.

Here, we utilize the Watson−Crick base pairing to tailor DNA nanopyramids (DP) and integrate both antimicrobial functionalities with bioimaging capabilities into a single DNA-based entity. The bioimaging capabilities enable us to assess the efficacy of antimicrobial compounds delivery in a theranostic manner. Actinomycin D (AMD) was chosen as a model antimicrobial

compound in our concept. AMD has been shown to inhibit DNA dependent RNA synthesis by binding to dsDNA template and in turn interfering with the RNA elongation process.[27,28] Because AMD can intercalate with dsDNA, we then used the DP to protect and stabilize AMD. Moreover, DP utilization would allow the normally impermeant AMD[29] to cross the cell membrane and to be delivered inside the cells. In addition, we conjugated red-emitting gold nanoclusters (Au NCs) on the apexes to detect and assess the efficacy of this nanotheranostic DNA structure. Our proof of concept study demonstrated that the nano-theranostic DNA structure design successfully delivered the antimicrobial compounds to two important commonly encountered bacteria, *Escherichia coli* (*E. coli*) and *Staphylococcus aureus* (*S. aureus*), as shown by the reduction in their log growth. In addition, conjugation of Au NCs on DP greatly increases the ease of assessing AMD delivery efficacy.

■ EXPERIMENTAL DETAILS

All chemicals were used as received. Ultrapure water was prepared from Millipore filtration unit (18.2 MΩ cm) and was used as universal solvent in this study. All glassware was washed with *aqua regia*, rinsed with ethanol and copious water, and dried in an oven before use.

Materials. *Bacteria Strains.* The bacteria strain of *Escherichia coli* K12 (*E. coli*; ATCC 700926) was purchased from ATCC (USA). The *Staphylococcus aureus* (*S. aureus*; ATCC 25923) was a kind gift from Prof Tan Kai Soo.

Oligonucleotide Strands. HPLC-purified oligonucleotides were ordered from Sigma-Aldrich (USA). The oligonucleotide sequences are listed as follows:

oligonucleotide	sequence
strand A	5′-ACA TTC CTA AGT CTG AAA CAT TAC AGC TTG CTA CAC GAG AAG AGC CGC CAT AGT A- 3′
strand B	5′-SH-C6-TAT CAC CAG GCA GTT GAC AGT GTA GCA AGC TGT AAT AGA TGC GAG GGT CCA ATA C-3′
strand C	5′-SH-C6-TCA ACT GCC TGG TGA TAA AAC GAC ACT ACG TGG GAA TCT ACT ATG GCG GCT CTT C-3′
strand D	5′-SH-C6-TTC AGA CTT AGG AAT GTG CTT CCC ACG TAG TGT CGT TTG TAT TGG ACC CTC GCA T-3′

Chemicals. Luria−Bertani (LB) and plate count agar powders were purchased from Becton Dickinson (USA). DNase I was obtained from Thermo Scientific (USA). Actinomycin D (AMD), dithiothreitol (DTT), ethidium bromide, ethylene diamine tetra acetic acid (EDTA), L-glutathione reduced (GSH), 4-*N*-(Maleimidomethyl)cyclohexane-1-carboxylic acid 3-sulfo-*N*-hydroxyduccinimide ester sodium salt (sulfo-SMCC), magnesium chloride (MgCl₂), SBYR Green, sodium borohydride (NaBH₄), and Tris base were purchased from Sigma-Aldrich (USA). Hydrogen tetrachloroaurate(III) hydrate (HAuCl₄· H₂O) was from Alfa Aesar. Tali viability kit-dead cell green was obtained from Life Technologies.

Methods. *DNA Nanopyramid Assembly, GSH-Au NCs Decoration, and Actinomycin D Loading.* DNA nanopyramid (DP) was self-assembled with slight modification from the previous report.[22] Briefly, DP stock (20 μM) was prepared by mixing an equimolar amount of four oligonucleotide strands in annealing buffer (20 mM Tris, 50 mM MgCl₂, pH 8.0). The mixture then was heated at 95 °C for 2 min followed by incubation in ice bath.

To achieve diagnostic properties, DP was subsequently decorated with GSH-Au NCs. Briefly, the DP which carries thiol moieties was introduced to 100 mM of DTT (1 h, room temperature) to fully reduce the thiol moieties. Following DTT pretreatment, the mixture was purified using spin column (Pierce; MWCO 30 000) ultrafiltration (15 000 × g for 15 min). Afterward, the mixture was washed twice with ultrapure water and the DP concentrate was then collected. Concurrently, 100 μM of GSH-Au NCs were activated with sulfo-SMCC cross-linker (4.8 mg/mL) for 1h at room temperature. Then, the

maleimide-activated GSH-Au NCs were purified with spin column (Pierce; MWCO 3,000) under centrifugation (15 000 × g for 15 min). The mixture then was washed twice with ultrapure water and the maleimide-activated GSH-Au NCs concentrate was collected. Thereafter, the DP concentrate and the maleimide-activated GSH-Au NCs concentrate were incubated for 3h under stirring at room temperature. The decoration took place via mediation of the maleimide structure bridging between the DPs' thiol groups and the amine moieties on the GSH coating of Au NCs. Following the incubation, the Au NCs decorated DP (DPAu) was purified and washed twice through spin column (Pierce; MWCO 30 000) under centrifugation condition of 15 000 × g for 15 min. The DPAu containing concentrate was collected.

Therapeutic moiety, AMD was let to intercalate into DPAu by incubating the mixture with ratio of AMD:DPAu = 100:1 in overnight stirring at 4 °C. Thereafter, the mixture was purified with spin column (Pierce; MWCO 3,000) under centrifugation (15 000 × g for 15 min). The mixture was washed twice with ultrapure water and the AMD-loaded DPAu (DPAu/AMD) concentrate was collected. Following purification step, the loading capacity of DPAu/AMD was calculated on the basis of the measurement of AMD and DNA concentration in the concentrate as shown in the following formula

$$\text{loading} = \frac{\text{mol AMD}}{\text{mol DP}}$$

AMD concentration was determined with Epoch microplate spectrophotometer (Biotek) at absorbance wavelength of 439 nm. Similarly, the amount of DNA was determined with absorbance measurement at 260 nm with microvolume Epoch spectrophotometer (Biotek).

DPAu/AMD Characterization. The hydrodynamic size and size distribution of DP, DPAu, and DPAu/AMD were measured by dynamic light scattering (DLS; Brookhaven, USA) in aqueous medium. The DP variants (3 μM, 10 μL) were prepared and were diluted to 50 μL using ultrapure water. The diluted DP variants were then centrifuged with speed of 13 000 × g at 4 °C for 1.5 h. The top 25 μL of the solution was collected and was further diluted to 600 μL prior to the measurement. For control experiment, single stranded DNA (ssDNA; strand B) with the same amount was also measured with the DLS. Additionally, DLS measurement was also conducted for the mixture of 4 strands of oligonucleotides (strands A, B, C, and D), which were mixed and kept in 4 °C, as not to allow the strands to hybridize and form DP structure.

The self-assembled DP and theranostic DPAu/AMD were dropped on glass slides and oven-dried (60 °C) prior to XPS analysis (AXIS HIS, Kratos Analytical) with a mono Al Kα radiation source (hν = 1486.71 eV) operating at 15 kV and 5 mA. The produced spectra were calibrated with internal standard C 1s peak of 284.5 eV. XPS spectra were deconvoluted with XPSPEAK 4.1 (http://www.uksaf.org/software.html). The peaks were assigned according to the literature.[30,31]

DPAu/AMD Uptake Study. Cellular uptake of the DPAu formulation was observed with confocal laser scanning microscopy (CLSM, Olympus Fluoview FV1000, Japan). DPAu with concentration of 0.75 μM was incubated with 1 × 10⁶ CFU/mL of *E. coli* or *S. aureus* in LB medium at 37 °C, 200 rpm. Afterward, the bacteria were collected and washed thrice with 1 × PBS with centrifugation (6000 × g, 2 min). The pellets were resuspended in 1 × PBS in an 8-well cover glass chamber (LAB-TEK, Nunc, USA). Finally, the bacteria were viewed with CLSM using 100× oil immersion objective lens.

The quantitative study of DPAu uptake into the bacteria was assessed by the microplate reader. Briefly, 0.75 μM of DPAu was mixed either with 1 × 10⁶ CFU/mL of *E. coli* or *S. aureus* in LB medium. The mixture was then distributed in 6 wells and was incubated at 37 °C, 200 rpm for 3 h. Following the incubation, the DPAu from the first set of 3 wells were removed and the bacterial cells were washed thrice with 1 × PBS and resuspended back in the LB medium; while the second set of 3 wells served as reference control wells and left as it was. The fluorescent intensities then were measured with a microplate reader (Tecan, Switzerland) at excitation wavelength of 670 nm and emission wavelength of 740 nm. The uptake efficiency was expressed as the percentage of the fluorescence of the testing wells over that of the reference control wells.

Theranostic DPAu/AMD Efficacy. The efficacy of theranostic DPAu/ AMD was assessed against 2 bacterial strains, *E. coli* and *S. aureus*.

The bacteria stock cultures were grown overnight from a single colony of each strain in LB medium at 37 °C, 200 rpm. Following overnight culture, the corresponding optical density at 600 nm was measured and it was determined that $OD_{600} = 1$ is equivalent to 3×10^8 CFU/mL and 1.5×10^9 CFU/mL of *E. coli* and *S. aureus*, respectively.

To determine the efficacy of DPAu/AMD against free AMD, the bacteria culture was seeded at initial seeding density of $3-4 \times 10^6$ CFU/mL and was treated with either DPAu/AMD or free AMD to give final AMD concentration of 100 μM. Both DPAu/AMD and free AMD addition were kept at fixed composition of 10 vol %. from total mixture volume. Ultrapure water with equal composition ratio was introduced as experimental control. The mixtures were grown for 8 h (200 rpm, 37 °C). At the end of incubation time, the cell mixtures were serial diluted, plated on plate count agars, and grown for an additional 18 h. Subsequently, the colonies were counted and the bacterial log growth could be determined with the following equations

$$\text{log growth} = \log \frac{(\text{cell number})_{\text{sample},t=8}}{(\text{cell number})_{\text{initial},t=0}}$$

$$\text{normalized log growth} = \frac{\text{log growth sample}}{\text{log growth control}}$$

The inherent capability of DPAu/AMD to detect the amount of dead bacteria was validated with commercially available live/dead cell stain, Tali dead cell green. Briefly, 1×10^6 CFU/mL of bacterial cells was treated with either DPAu/AMD (final AMD concentration of 100 μM) for 2 h. Following the exposure the bacteria were collected and washed thrice $1 \times$ PBS with centrifugation ($6000 \times$ g, 2 min). The pellets were suspended in $1 \times$ PBS and stained with Tali dead cell green as per supplier's instruction. Afterward, the bacteria cells were added into an 8-well cover glass chamber (LAB-TEK, Nunc, USA) and were viewed with CLSM using $100\times$ oil immersion objective lens. In order to quantify the DPAu capability to indicate bacterial cell death, signals from both red (DPAu) and green (Tali dead cell green) were analyzed for overlapping signals with ImageJ. The signals bivariate analysis and the overlap coefficient (R) were generated from the ImageJ's colocalization inbuilt plugin following previous reports.[32,33] Overlap coefficient is defined as the number of signals from both channel that colocalized, with $R = 1$ as the highest colocalization degree.[32,33]

AMD Release Mechanism. DPAu was incubated with DNase I (2, 5, 10 U) at 37 °C for 30 min. Following the incubation, the reaction was terminated with the addition of 5 mM EDTA. Subsequently, $2 \times$ SBYR Green solution in TE buffer (10 mM Tris, 1 mM EDTA, pH 8.0) was added into the mixture with ratio of 1:1. The melt curve and melt peak were measured with CFX96 Real Time system (Biorad).

To quantify the degree of AMD being released from the DNA nanopyramid structure, DPAu/AMD was incubated with different concentration of DNase I (2, 5, 10 U) at 37 °C for 30 min. Afterward, the reaction was terminated with 5 mM EDTA and the reaction mixture was spin trough purification column (Pierce; MWCO 3,000) under centrifugation (15 000 $\times$g, 15 min). The supernatant was collected and the amount of AMD being released from the DPAu structure was determined by A_{439} measurement of the supernatant. The Act D amount in the supernatant were normalized against its initial concentration and the normalization value was reported. Similarly, the amount of DNA being degraded was determined by measuring the oligonucleotide content in the supernatant. The oligonucleotide content was measured with absorbance of 260 nm with Epoch microvolume spectrophotometer (Biotek). The measured concentration of oligonucleotide in the supernatant then was normalized against its DPAu initial concentration. The normalized value was reported.

Statistical Analysis. All experiments in this study were done in triplicate. Data are mean $\pm$ standard deviation (SD). The statistical significance were ascertained following Student's *t*-test with significant level of $p < 0.05$.

RESULTS AND DISCUSSION

To achieve a theranostic outcome, we designed the DP to carry ultrasmall red emissive Au NCs, which were produced as described in previous report,[34] but with AMD payload tightly integrated and protected within the DP. Ultrasmall Au NCs were chosen as their small sizes bring about a unique photoluminescent property observed when these unique subclass of gold-based nanomaterials decrease to sizes of less than 2 nm.[34−36] Moreover, our previous study showed that these Au NCs were innately safe, as they induced minimal cytotoxic effects.[37] The ultrasmall red emissive Au NCs were obtained by synthesizing clusters that consist of about 25 gold atoms in their cores. These cores were protected by a monolayer of thiolate ligands that are derived from glutathione (GSH) addition, resulting in the formation of GSH-Au NCs with a core size of ∼1.5 nm (see Figure S1 in the Supporting Information). This size is in line with what we have reported previously where in which the GSH-Au NCs were found to be with core size of 1.4 nm.[34] Our XPS analysis further confirmed the formation of GSH-Au NCs. High resolution scanning showed the doublet peak of Au 4f at binding energy of 84.4 and 88.2 eV (see Figure S2 in the Supporting Information), which corresponds to Au $4f_{7/2}$ and Au $4f_{5/2}$, respectively.[38,39] The photoluminescence properties of the synthesized GSH-Au NCs showed that the Au NCs absorb the light at about 670 nm (see black line in Figure S3 in the Supporting Information) and in turn produced red emission at about 740 nm (see red line in Figure S3 in the Supporting Information). Visual observation of the GSH-Au NCs revealed that the brown Au NCs (see inset left panel in Figure S3 in the Supporting Information) emitted strong red fluorescence under UV illumination (see inset right panel in Figure S3 in the Supporting Information).

Having the GSH-Au NCs successfully prepared, we carried on the study with the formation of DNA nanopyramids (DP). The Watson and Crick base pairing allows the four oligonucleotides (see oligonucleotide sequences listed in experimental section) to self-assemble in the form of DP structure (Figure 1). Three of the strands carried thiol groups at their 5′ ends, resulting the DP structure, which when successfully assembled, to carry three thiol groups at the base of the structure. These thiol groups were utilized to attach the GSH-Au NCs onto the structure which were facilitated by Sulfosuccinimidyl-4-[N-maleimidomethyl]-cyclohexane-1-carboxylate (sulfo-SMCC). Sulfo-SMCC was needed as the red emissive Au NCs used in this study were protected by peptide (GSH). Though, the GSH ligand is necessary to stabilize the Au NCs, its protective presence means that the gold surface is not readily available for conventional thiol mediated conjugation strategy.[22] Sulfo-SMCC conjugation occurred via mediation of maleimide structure acted as cross-linker between the thiol groups and the amine groups in the GSH-Au NCs, resulting in the formation of Au NCs conjugated DNA nanopyramids (DPAu).

Building from this DPAu framework, we incorporated the therapeutic biomolecules, AMD, through exploiting insertion chemistry of its phenoxazone aromatic rings parallel to the guanine base of DNA. This strongly lodges the two cyclic pentapeptide of AMD in the DNA minor groove and overall intercalates the drug to the DPAu framework.[28,40] We found that we could incorporate approximately 49 molecules of AMD in one DPAu structure. This loading ratio was in close approximation with the theoretical loading value, which could be estimated on the basis fo the guanine base motif in the DP structure (51 guanine bases). With this successful incorporation of AMD

21824

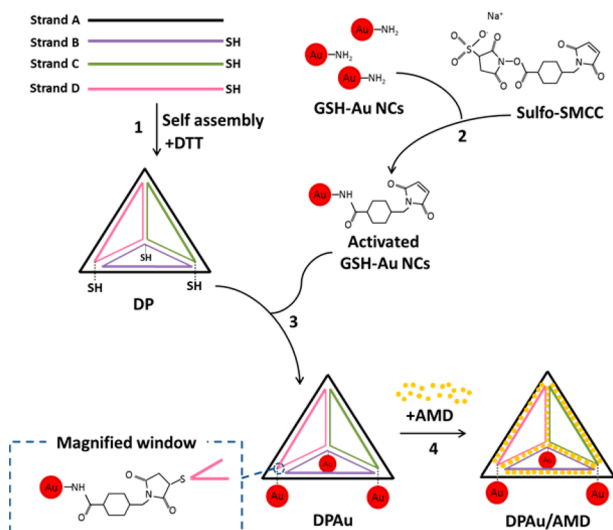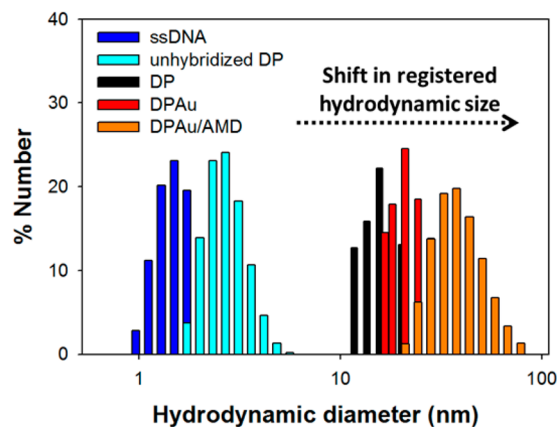dx.doi.org/10.1021/am502591c | *ACS Appl. Mater. Interfaces* 2014, 6, 21822−21831

Figure 1. Schematic representation of nanotheranostic DPAu/AMD synthesis. (1) DNA nano pyramid (DP) is self-assembled from four complementary oligonucleotides and DTT is added to fully reduce the thiol groups on the DP. (2) At the same time, GSH-protected Au NCs are activated with sulfo-SMCC to allow (3) the conjugation of Au NCs on the DP (DPAu) via maleimide bonds (magnified window). (4) Then, the Actinomycin D (AMD) is let to intercalate into the DPAu structure and the nanotheranostic DPAu/AMD structure is formed.

Summary of physical characterization of nanotheranostic DP, DPAu, DPAu/AMD

	Size (nm)	Polydispersity (PDI)
ssDNA	1.15 ± 0.27	0.67 ± 0.17
Unhybridized DP	3.16 ± 0.69	0.44 ± 0.23
DP	15.7 ± 2.65	0.17 ± 0.06
DPAu	21.0 ± 3.41	0.28 ± 0.02
DPAu/AMD	38.3 ± 4.21	0.23 ± 0.05

Figure 2. Characterizations of DP, DPAu, and DPAu/AMD. The histogram shows the registered size distribution of structure is significantly shifted to a higher size range when the DP nanostructure was formed. In addition, with more moieties added on the DP structure, the registered hydrodynamic size shifted further to bigger size range. ssDNA = single-strand DNA (strand B); unhybdridized DP (mixture of strands A, B, C, D); DP = DNA nanopyramid; DPAu = Au NC-conjugated DNA nanopyramid; DPAu/AMD = Au NC-conjugated DNA nanopyramid loaded with AMD. Lower panel: summary of physical characterization of nanotheranostic DP and DPAu obtained from dynamic light scattering (DLS) analysis. Data are mean ± SD, $n = 3$.

into the DPAu structure, we obtained the nanotheranostic DPAu/AMD (Figure 1).

Characterization of Self-Assembled Theranostic DNA Nanopyramid Structures. The assembled DNA nanopyramid was characterized by native polyacrylamide gel electrophoresis (PAGE). Figure S4A in the Supporting Information shows that DP structure moved at slower rate, when compared to other mixtures of single-stranded DNA (see lane 5 in Figure S4A in the Supporting Information) or combination of two (see lane 3 in Figure S4A in the Supporting Information) or three strands (see lane 2 in Figure S4A in the Supporting Information). This further confirmed the successful synthesis of the nanopyramid.[22] In addition, slower migration rate could be detected with additional moieties on the DP (see Figure S4B in the Supporting Information). Native PAGE analysis shows that DPAu and DPAu/AMD migrate slower than their DP counterpart. This could be due to the increase in the nanostructures' overall size and charge.

The DLS analysis resulted in the registered DP hydrodynamic size of 15.7 nm (Figure 2). It is worth noting that the registered hydrodynamic size reported here is significantly bigger than the expected DP size of 6.12 nm. This could be attributed to the fact that hydrodynamic size from DLS analysis was derived based on the light scattering of particles with basic assumption that they are spherical in shape. This assumption allows the application of Stokes−Einstein equation[41] to employ the particle translational diffusion coefficient to obtain the particle hydrodynamic size. However, because of the anisotropic pyramidal configuration, DP rotational diffusion coefficient also plays a role. This is made obvious because with different rotation position of the DP structure (i.e., whether the light shine on the lateral side of the DP or on one of its vertex), different light scattering profile will be registered. In addition, curvature of the double helix will also attribute to different light scattering profile. Thus, the overall registered hydrodynamic size that we obtained was more likely to be the diameter of spherical particle that possess the same translational diffusion speed coefficient to obtain the particle hydrodynamic size.

Though the apparent hydrodynamic size data is only an approximation of the DP structure, it can be used to assess the formation and modification of DP structure. Our control experiment showed that single-stranded DNA (ssDNA; modeled by strand B) gave an apparent hydrodynamic size of 1.15 nm. Moreover, the hydrodynamic size of unhybridized DP (4 strands mixture) was registered at 3.2 nm. Interestingly, the registered hydrodynamic size increases significantly when the same mixture was allowed to hybridize, indicating the formation of DP. These results were in good agreement with our aforementioned PAGE analysis (see Figure S4 in the Supporting Information). The initial DP size shifted further with each addition of moieties (Figure 2). Au NCs conjugation added about 5 nm to the structures' overall registered hydrodynamic size. Similarly, we noted that AMD loading onto the scaffold structure resulted in the 18 nm increase on the overall nanotheranostic's hydrodynamic size. We reckon this dramatic increase in the overall hydrodynamic size was caused by the way AMD intercalates to the DP scaffold, because AMD intercalates by inserting its phenoxazone aromatic rings parallel to the guanine base of DNA. This mode of intercalation leaves the majority of the drug compound to protrude out of the scaffold, adding to the overall hydrodynamic size.

To confirm the incorporation of Au NCs and AMD to our DP structure, we conducted XPS analysis of the DNAu/AMD. Our XPS analysis (Figure 3) detected the presence of signal for C 1s, N 1s, O 1s, P 2p, and S 2p on both DP and DPAu/AMD
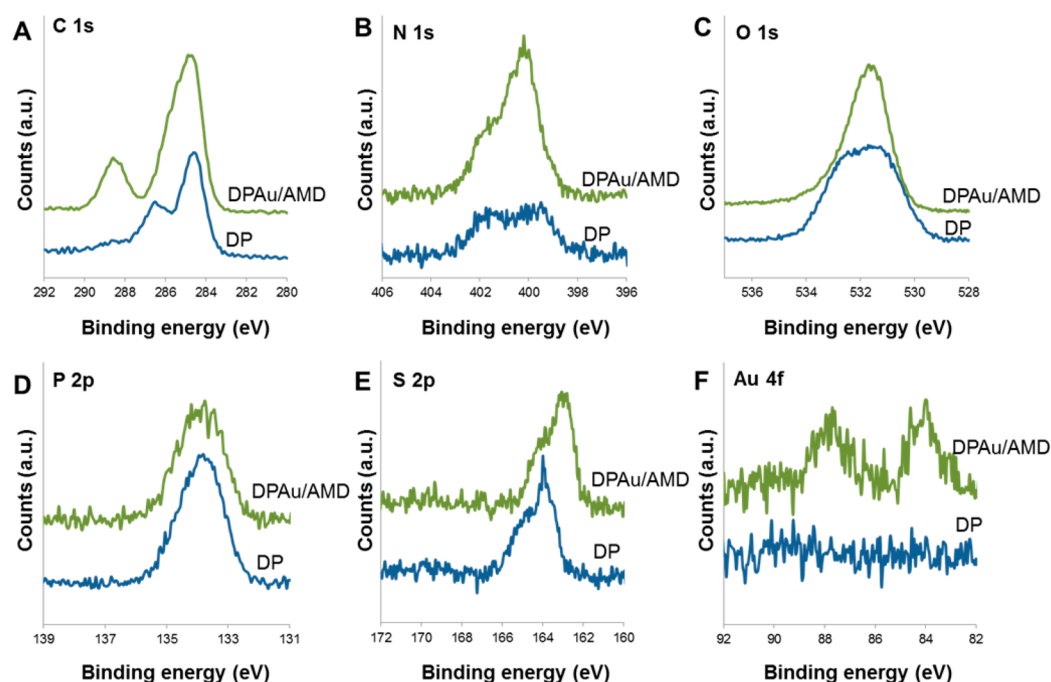
Figure 3. XPS high-resolution scanning of DP and DPAu/AMD. Samples were scanned for elements of (A) C 1s, (B) N 1s, (C) O 1s, (D) P 2p, (E) S 2p, and (F) Au 4f. DP signals were indicated in blue and DPAu/AMD signals were indicated in green.

Table 1. Summary of Peak Assignment Obtained from XPS Spectra Deconvolution of Nanotheranostic DPAu/AMD

signal peak		peak assignment	DP		DPAu/AMD	
			B.E. (eV)	relative atomic percentage (%)	B.E. (eV)	relative atomic percentage (%)
C 1s	C1	C−C, C−H	284.5	38.4	284.5	20.8
	C2	C−N, C−O	285.2	21.8	285.1	45.0
	C3	N−C(=O)−C, N−C(=N−N), N(=C)−N	286.6	34.5	285.9	15.0
	C4	O−C−OH, O=C−N	288.6	5.3	288.5	19.2
N 1s	N1	N−C, N−H (unprotonated amine)	399.7	60.4	399.8	76.2
	N2	N−H (protonated amine)	401.7	39.6	401.4	23.8
O 1s	O1	C−OH, P−O (Phosphate)	531.6	69.7	531.1	49.9
	O2	C=O	532.6	30.3	532.6	50.1
P 2p	P1	P−O	133.5	100.0	133.4	100.0
S 2p	S1	S−H	163.8	100.0	162.9	100.0
Au 4f	Au1	Au^0			84.1	100.0

structures. From the many elements scanned, the P 2p signal belongs uniquely to the DNA, the base materials for our nanotheranostic construct in this study. Consistently, the P 2p signal that appears at a binding energy of 133.5 eV could be observed on both DP and DPAu/AMD structures (see Table 1 and Figure S5 in the Supporting Information). This P 2p peak signals for the presence of phosphate groups of the DNA backbone. Corresponding O 1s spectra deconvolution of DP sample revealed the presence of P−O bonds, which overlapped with C−OH signal peaks and centered at binding energy of 531.6 eV. Moreover, DNA characteristic peaks could be observed on the DP structure. C 1s scanning (see Table 1 and Figure S5 in the Supporting Information) revealed the presence of C−C and C−H (284.5 eV), C−N and C−O (285.2 eV), N−C(=O)−C, N−C(=N)−N, and N(=C)-N (286.6 eV), in addition to O−C−OH and O=C−N (288.6 eV) bonds. These bonds could be attributed mainly to the sugar base and the nitrogen base of the DNA.[42] Correspondingly, the deconvolution of N 1s spectra of DP structure revealed the presence of N−C and unprotonated amine groups centered at 399.7 eV while the protonated amine

groups centered at 401.7 eV.[42] This N 1s signals were contributed by the nitrogen base compounds of the DNA, the purines and the pyrimidines. The presence of thiol groups was ascertained with S 2p scanning, which gave the characteristic peak at 163.8 eV.[43]

The success of Au NCs incorporation onto the DNA structure was ascertained by the presence of doublet Au 4f signal peaks on DPAu/AMD but not on DP structure (Figure 3). This doublet peaks corresponds to Au 4f$_{7/2}$ and Au 4f$_{5/2}$ at approximately 84.1 and 87.9 eV, respectively (see Table 1 and Figure S5B in the Supporting Information).[38,39] The Au 4f peaks signal for Au^0 and was consistent with the XPS spectra obtained for GSH-Au NCs (see Figure S2 in the Supporting Information). S 2p scanning of DPAu/AMD structure (see Table 1 and Figure S5 in the Supporting Information) revealed that the thiol peak shifted by approximately 0.9 eV. This shift could be attributed to the binding of the Au NCs to the DP structure.[43]

The incorporation of AMD to the DPAu structure could be observed by the overall increase of the C 1s, N 1s and O 1s signals from the DPAu/AMD XPS spectra (Figure 3). In addition to the

overall signal increase, the composition of the peaks changed with the incorporation of AMD. Deconvolution of C 1s spectra of DPAu/AMD (see Table 1 and Figure S5B in the Supporting Information) revealed that C−N and C−O (285.1 eV) in addition to O−C−OH and O=C−N bonds (288.5 eV) became major species in the C 1s spectra. Likewise, amide and unprotonated amine group became the prevailing species in the N 1s, while C=O bond dominated the O 1s spectra (Table 1). This increase in signals came from AMD's carboxylic and amine groups, which in turn increased the amount of amide bonds being detected in DPAu/AMD structure.

DPAu Uptake Study. As AMD mode of action is blocking the RNA synthesis, which occurs intracellularly, the efficacy of the nanotheranostic DPAu/AMD constructs hinges on the success uptake of the nanostructure inside the infectious bacterial cells. Figure 4A shows confocal images of E. coli and S. aureus
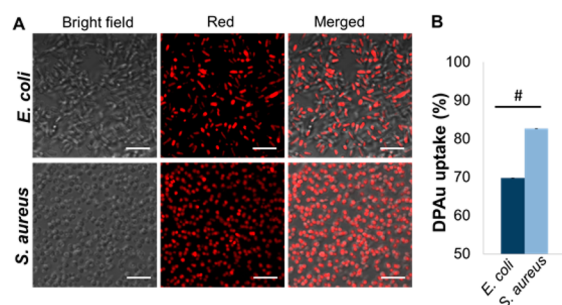

Figure 4. Nanotheranostic DPAu was internalized by bacterial models. (A) Representative confocal laser scanning microscopy (CLSM) images show that both E. coli and S. aureus could uptake of the DPAu (3 h incubation). Bright-field channel shows total bacteria cells; Red channel shows the red fluorescence signal from Au NC tagged on the DP structure. Experiment was conducted in triplicate. Scale bar: 5 μm. (B) Quantification analysis shows that S. aureus is more efficient in uptaking DPAu structure. Data are mean ± SD, n = 3. #significant when compared to E. coli. One-tailed Student's t-test, p < 0.05.

bacteria after 3 h incubation with DPAu. The red fluorescence is emitted from GSH-Au NCs. From the images, it can be seen that our DPAu nanocarriers have been internalized into the bacteria cytoplasm. The intensity of red fluorescence indicated the number of DPAu that have been internalized into the bacteria as all the images were taken under the same setting from the same confocal microscope. The observation of the uptake was further confirmed by fluorescence intensity quantification with microplate reader. From Figure 4B, we noted that the uptake efficacy of

S. aureus is 1.2 fold higher than that of E. coli. We reckon that the particles internalization in the bacterial cells could be eased by the DPAu nanocarrier's small size and pyramidal shape.

Efficacy of Nanotheranostic DPAu/AMD in Combating Bacterial Infection. To assess the drug delivery ability of nanotheranostic DPAu/AMD, we chose two bacterial strains, E. coli and S. aureus, which represent Gram-negative and Gram-positive groups, respectively. Our result showed that both DP and DPAu structures did not exert any killing effect on the tested bacterial strains (see Figure S6 in the Supporting Information). Instead using the DPAu/AMD structure brought about a dose dependent killing effect on both E. coli and S. aureus cells. In addition, our result indicates that AMD packaged in DPAu show a significant killing effect of the bacteria when compared to the free AMD treatment. We observed 100 μM of free AMD achieved 42% cell population reduction while the same amount of AMD (100 μM) packaged in DPAu structure (DPAu/AMD) enhance the killing effect yielding the final reduction of 65% of total S. aureus population (Table 2). Similarly, packing AMD into the DPAu structure was shown to be beneficial in the E. coli cell system, as evidenced by a heightened killing effect enhancement from 14% of cell reduction for free AMD to 48% of cell reduction for DPAu/AMD (Table 2). It has been suggested that the optimum radius of nanostructure for drug delivery to be 25 nm, as the nanostructure in this size range induce high cell uptake.[44,45] Considering the DPAu/AMD's hydrodynamic size lies within this optimum size range (38 nm, Figure 2), we reckoned that the killing effect enhancement could partially be related to the higher uptake of DPAu/AMD into the cells when compared to the passively diffusing free AMD (~0.12 nm).

We observed that both E. coli and S. aureus were responding to the DPAu/AMD treatment, as evidenced by the reduced number of viable cells left after the exposure. This suggests that DPAu/AMD could be applied to treat a broad spectrum of targets. Though both model bacterial strains are susceptible to the nanotheranostic DPAu/AMD exposure, S. aureus shows higher susceptibility to the treatment. This could be caused by the inherent differences in the bacterial cell membrane superstructure between both bacterial strains. S. aureus possesses a single cell membrane, whereas in comparison, E. coli possesses an additional outer membrane.[46,47] This additional outer membrane may pose as additional barriers for DPAu/AMD transport across the E. coli membrane.[45] Moreover, it has been reported that Gram-positive bacteria possesses approximately 30 DNA binding sites per cell, whereas the Gram-negative group has 4−8 DNA binding sites per cell, resulting in different DNA material uptake

Table 2. Efficacy of Nanotheranostic DPAu/AMD in Combating Bacterial Infection[a]

	concentration (μM)	E. coli			S. aureus		
		cell number (CFU/mL)	log growth	normalized log growth	cell number (CFU/mL)	log growth	normalized log growth
initial		2.90×10^{06}			4.33×10^{06}		
control		2.56×10^{11}	4.95	1.00	4.90×10^{11}	5.00	1.00
AMD	1	3.13×10^{11}	5.02	1.02	2.10×10^{11}	4.68	$0.94^{b,d}$
	10	8.57×10^{10}	4.47	0.90^{b}	4.67×10^{10}	3.95	$0.79^{b,d}$
	100	5.50×10^{10}	4.28	0.86^{b}	4.10×10^{09}	2.90	$0.58^{b,d}$
DPAu/AMD	1	2.77×10^{11}	4.98	1.01	2.13×10^{11}	4.63	$0.93^{b,d}$
	10	3.43×10^{10}	4.07	$0.82^{b,c}$	1.93×10^{09}	2.63	$0.52^{b,c,d}$
	100	1.13×10^{09}	2.59	$0.52^{b,c}$	3.67×10^{08}	1.76	$0.35^{b,c,d}$

[a]Data represent the mean of three independent experiments. [b]significant against untreated control. [c]significant against free AMD treatment. [d]significant against E. coli. One-tailed Student's t-test, p < 0.05.

rate between these two bacterial groups.[46] All these factors could be used to explain the differential uptake of DPAu/AMD in *E. coli* and *S. aureus*, which in turn resulted in the differential drug delivery efficacy effect exerted on the two strains.

Thus far, we intuitively understand that the DPAu/AMD uptake is essential for the drug to take effect. To validate our understanding, we took the DPAu/AMD treated bacterial cells and stained them with a commercial nucleic acid stain, Tali dead cell green. As the Tali dead cell green stain is impermeant toward cell membrane, it can be used to discriminate the live and dead bacterial cells,[48] further validating our Au NCs signals. Our results show that following 2 h exposure to DPAu/AMD, majority of bacterial cells had internalized the nanotheranostic structure, as evidenced by the red fluorescence signals emitted from the Au NCs (Figure 5A). Our Tali dead cell green staining
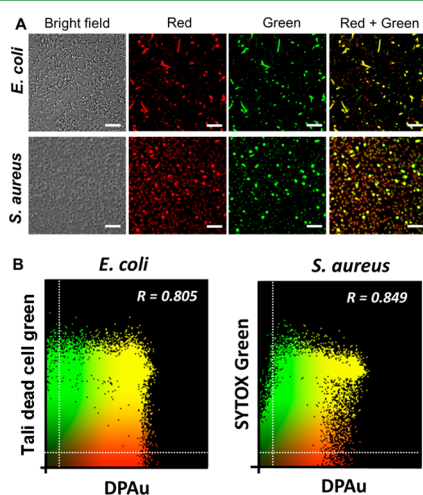

Figure 5. Evaluation of nanotheranostic DPAu/AMD performance. DPAu/AMD needs to be taken in by the cells for effective killing effect. (A) DPAu/AMD-treated *E. coli* and *S. aureus* cells were stained with live/dead cell stain, Tali dead cell green, for validation of killing effect. CLSM images showed that cells took in the DPAu/AMD structure, as evidenced by the red fluorescence of Au NCs. This DPAu/AMD internalization resulted in cell death, as evidenced by the overlapping signals from Tali dead cell green and Red Au NCs (Red + Green = Yellow). Bright field showed total bacterial cells; Red channel indicates cells containing theranostic DPAu/AMD; Green channel (Tali dead cell green) signals for dead bacterial cells. Scale bar: 10 μm. (B) DPAu/AMD structure killing efficacy could be directly assessed by the presence of its red fluorescence signals from conjugated Au NCs. Bivariate analysis of DPAu and Tali dead cell green fluorescence signals suggested good correlation of Au NCs signals with the commercial live/dead stain in assessing bacterial cell death, as evidenced by the signal colocalization and high overlap coefficient (R). Green: Tali dead cell green signals. Red: DPAu signals. Yellow: Overlap signals. Dotted lines show the signal threshold. Images presented are representative of three individual experiments.

confirmed that this uptake was truly essential for killing the infectious bacterial cells. Consistently, we observed that the majority of those bacteria which took in the DPAu/AMD structure were stained positive for Tali dead cell green, as evidenced by the signal overlap from Tali dead cell green and Au NCs when both channels were merged.

In addition, our bivariate analysis of Tali dead cell green and Au NCs signals show a high degree of signal overlapping (yellow dots; Figure 5B). In addition, our analysis showed both bacteria models had a Mander's overlap coefficient (*R*) value greater than

0.8, indicating good correlation of both signals. This suggests that Au NCs signals which were inherently generated from the DPAu/AMD structure itself is sufficient to indicate bacterial cells death and could potentially be used to assess the efficacy of drug delivery. It is worth noting that not all signals overlap. For example, we could detect dead cells that did not carry any DPAu signals (green dots, Figure 5B). We reckon this could be caused by the inherent dead cell population that could be found in any bacteria culture.

AMD Release Mechanism from DPAu/AMD. For a bioactive compound bound to its trans-membrane carrier to work, it has to be released from its vehicle. This brings us to one of the fundamental questions in this study of how the AMD was released from its carrier, DPAu. It has been suggested that the intercalated drug release from DNA nanostructure is facilitated by the environment pH.[19] Kim et al. reported a significant release of doxorubicin after 10 h incubation at pH 5 buffer solution due to partial disassembly of the DNA structure, while minimum drug release could be observed in physiological pH (pH 7.4) condition.[19] This proposed mechanism is intuitively not applicable for our case, as prokaryotic cells, unlike the mammalian cells, do not possess endosome/lysosome compartments in which the acidic pH (pH 5) could be exerted. Both *E. coli* and *S. aureus* maintain their intracellular pH at the range from pH 7.2 to 7.8 at all time, to preserve enzyme activity, as well as protein and nucleic acid.[49,50] On the basis of the proposed mechanism by Kim et al., supposedly there would be a minimum AMD release from the DPAu structure as the bacteria's intracellular pH is not conducive for its release. However, this is counterintuitive with our observed DPAu/AMD killing effect which suggests that the AMD was successfully released from the DPAu. Altogether, these evidence further highlighted that AMD release from the DP was not a pH mediated process. To understand the mechanism of AMD release, we look no further than to the base material of this drug carrier. As the nanostructure was tailored from DNA as base material and both *E. coli* and *S. aureus* are known to possess abundant deoxyribonuclease (DNase) as part of their innate capability to attain transformation,[51−53] we hypothesized that the release of AMD from the DPAu structure was mediated by DNase.

In in vitro experiments, we introduced different amounts of DNase I into the DPAu nanostructure and observed that there was a dose dependent degradation of DPAu nanostructure with the increase of DNase I amount. The DPAu degradation could be observed from the significant loss of fluorescent signal from the intercalative dye SBYR green (Figure 6A), signifying the loss of initial dsDNA structure in the DPAu. Further proof of DNase I mediated degradation could be obtained from the melt peak analysis which showed the decrease of DPAu melting temperature from its initial value of 70 °C to final melting temperature of 33 °C at the highest tested DNase I concentration (Figure 6B). These results suggest that DNase I possess the capability to degrade the DP structure. We further hypothesized that through this DNase I mediated degradation, the AMD gets released from its interacting partner, DPAu and free to intercalate with bacterial DNA to exert its killing effect. To prove this, we mimicked the release of AMD from DPAu/AMD structure by incubating DPAu/AMD with DNase for 30 min and isolated the free AMD from the mixture with a spin column. Our observation showed that our control (DPAu/AMD only) lost a minimal amount of AMD, and with the increased amount of DNase I being introduced into the mixture, increased concentration of AMD could be found in the flow-through (Figure 6C). Correspondingly, increasing the DNase I amount resulted in an increasing
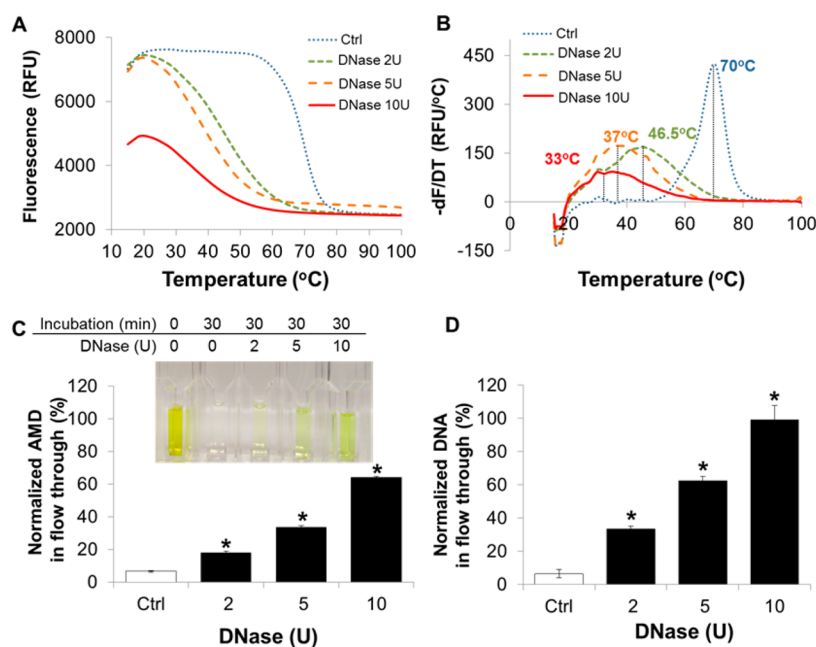
Figure 6. AMD release mechanism from nanotheranostic DPAu/AMD. The release of AMD from nanotheranostic structure was supposedly mediated by the degradation of DPAu structure cause by intracellular DNase. (A) Melt curve analysis and (B) melt peak analysis of nanotheranostic DPAu show the dose dependent degradation of DPAu's and decrease of melting temperature following DNase I ex vivo exposure (30 min). (C) Increase amount of AMD could be found in the filtration flow through following DNase I ex vivo exposure (30 min). Upper panel: Increase of AMD concentration in flow through could be detected by the increase of the color intensity in the flow trough. Data is mean $\pm$ SD, $n = 3$, *significant against control. Student's t-test, $p < 0.05$. (D) Similarly, increase of DNA amounts can be detected in the flow through with the increase of DNase I exposure (30 min). Data are mean $\pm$ SD, $n = 3$, *significant against control. Student's t-test, $p < 0.05$.

amount of DNA being detected on the flow through, suggesting the digestion of DPAu structure (MW ~68 kDa) into much smaller structure (<3 kDa). It is interesting to note that total degradation of the DPAu structure could be completed within 30 min time under the administration of 10 U DNase I. This rapid degradation is ultimately beneficial for combating bacterial infection, as the released drug could act and quickly curb the infection within one bacterial life cycle (doubling time 20−30 min), stemming the spread of bacterial infection. DNase I is known to target dsDNA, and our in vitro result suggested this cleavage by DNase I was sufficient to release the AMD from our unusual form of dsDNA. In the in vivo bacterial cytoplasm, there are other bacterial endonucleases that could even work in concert to degrade the DPAu/AMD structure and releasing the AMD in faster rate. It is also worthy to note that the real level of DNase I in the typical bacterial cells is much higher than the one that we introduced in the ex vivo study. On the basis of our meta-analysis (see the Supporting Information) from the reported bacterial DNase I level of activity in *E. coli*[53] and *S. aureus*,[54] we deduce that the amount of bacterial DNase would exceed even the highest concentration of DNase I that we used (10 U) by approximately 260 fold. This suggested that even more rapid degradation and AMD release could be expected in real bacterial infection case.

Overall, these results supported our initial hypothesis of AMD release mechanism is facilitated by DNase mediated degradation of its nanocarrier, DPAu. We propose the release mechanism as follow: (1) the release of intercalated AMD from its carrier DPAu is initiated with the uptake of nanotheranostic DPAu/AMD into the bacterial cells. (2) Following the uptake, the DPAu/AMD is rapidly degraded by the ubiquitous DNase, resulting in the release of AMD from the DPAu structure. (3) The free AMD then intercalate with its target, bacterial DNA, and exerts its antimicrobial effect.

Although we do not incorporate any targeting moieties in our current design, we could still exploit the subtle distinctions between mammalian cells and bacterial cells to ensure an efficient nanotheranostic performance of our design. One of the distinctions that could be made use in delivering the DPAu/AMD into the target bacterial cells is the innate competence of the bacteria to recognize and transport DNA materials across their cell membrane via mediation of DNA receptor protein (ComE family protein).[45] Moreover, once recognized, the DNA uptake rate into the cells is exhilaratingly fast, where in which 500−1000 nucleotide per second could be taken into the bacteria.[45] This suggests that even without any specific bacteria targeting capability, DPAu/AMD could still be transported into the bacteria in a rapid manner, ensuring killing efficacy in broad spectrum bacterial group. Rapid uptake to bacterial cells also offers the additional distinct advantage when this platform is used to combat bacterial infection in mammalian cells, as it could ensure that DPAu/AMD to escape AMD release in mammalian cells' cytoplasm. Another distinction could be observed in the localization of DNase in mammalian and bacterial cells. Bacterial DNase can be found in their cell membrane,[51,52] whereas mammalian cells' DNase is isolated in their nucleus and mitochondria.[55,56] This distinction would help to protect the DPAu/AMD from nuclease degradation while being in transit in mammalian cells; avoided unintended release of the drug cargo in cells and thus reduced potential cytotoxicity to the mammalian cells.

CONCLUSION

In conclusion, we have prepared a theranostic DNA nanopyramid structure which contains the diagnostic Au NCs in addition to the therapeutic AMD, namely DPAu/AMD. The nanotheranostic DPAu/AMD was observed to be readily taken

in by the *E. coli* and *S. aureus* and exerted its killing effect on them, suggesting that this structure is a good platform to treat and detect broad spectrum bacterial infection. The rapid intracellular degradation of DPAu/AMD, which could be mediated by DNase I, is fundamentally necessary in order to release the AMD from the structure. As DNA is natively present in any living cells, DNA by itself is noncytotoxic and biocompatible once it has done its job to deliver the drug to combat the bacterial infection. Overall, the DPAu/AMD is potentially a good platform for nano-theranostic approach to combat bacterial infection.

Future work could be dedicated to optimize the loading ratio of AMD into the DP structure. As AMD intercalation specifically target NpG or GpN steps (nucleotide- phosphate-guanine or guanine-phosphate-nucleotide) in dsDNA, DP sequence could be tailored to carry more of these intercalation sites. Thus, increasing the amount of AMD being incorporated in the DP structure, and in turn drive higher bacterial killing effect. In addition, we believe the next challenge to overcome in order for us to fully utilize this DNA-based nanotheranostic platform to combat bacterial infection lies in the better design of the DP to escape the endosomes of the bystander mammalian cells.

■ ASSOCIATED CONTENT

ⓢ Supporting Information

Additional characterization data on Au NCs and self-assembled DP can be found in the Supporting Information. This material is available free of charge via the Internet at http://pubs.acs.org.

■ AUTHOR INFORMATION

Corresponding Authors

*E- mail: cheltwd@nus.edu.sg. Phone: 65-65167262. Fax: 65-67791936.
*E-mail: chexiej@nus.edu.sg. Phone: 65-65161067. Fax: 65-67791936

Author Contributions

[†]M.I.S. and R.V.K. contributed equally, and designed and carried out the DNA nanopyramids experiments. X.Y. synthesized the gold nanoclusters. M.I.S., R.V.K., and D.T.L. conceived the hypotheses and concepts. M.I.S., R.V.K., C.Y.T., J.X., and D.T.L. performed analysis and wrote the paper. All authors read and approved the final manuscript.

Notes

The authors declare no competing financial interest.

■ ACKNOWLEDGMENTS

■ REFERENCES

(1) Abeylath, S. C.; Turos, E. Drug Delivery Approaches to Overcome Bacterial Resistance to Beta-lactam Antibiotics. *Expert Opin. Drug Delivery* **2008**, *5* (9), 931−949.

(2) Zhang, L.; Pornpattananangku, D.; Hu, C. M.; Huang, C. M. Development of Nanoparticles for Antimicrobial Drug Delivery. *Curr. Med. Chem.* **2010**, *17* (6), 585−594.

(3) Wang, X.; He, F.; Li, L.; Wang, H.; Yan, R.; Li, L. Conjugated Oligomer-Based Fluorescent Nanoparticles as Functional Nanocarriers for Nucleic Acids Delivery. *ACS Appl. Mater. Interfaces* **2013**, *5* (12), 5700−5709.

(4) Sun, J.; Chao, J.; Huang, J.; Yin, M.; Zhang, H.; Peng, C.; Zhong, Z.; Chen, N. Uniform Small Graphene Oxide as an Efficient Cellular Nanocarrier for Immunostimulatory CpG Oligonucleotides. *ACS Appl. Mater. Interfaces* **2014**, *6* (10), 7926−7932.

(5) Li, J.; Fan, C.; Pei, H.; Shi, J.; Huang, Q. Smart Drug Delivery Nanocarriers with Self-Assembled DNA Nanostructures. *Adv. Mater.* **2013**, *25* (32), 4386−4396.

(6) Kutty, R. V.; Feng, S. S. Cetuximab Conjugated Vitamin E TPGS Micelles for Targeted Delivery of Docetaxel for Treatment of Triple Negative Breast Cancers. *Biomaterials* **2013**, *34* (38), 10160−10171.

(7) Ma, X.; Zhao, Y.; Ng, K. W.; Zhao, Y. Integrated Hollow Mesoporous Silica Nanoparticles for Target Drug/siRNA Co-Delivery. *Chem. - Eur. J.* **2013**, *19* (46), 15593−15603.

(8) Zhang, W.; Meng, J.; Ji, Y.; Li, X.; Kong, H.; Wu, X.; Xu, H. Inhibiting Metastasis of Breast Cancer Cells *In Vitro* using Gold Nanorod-siRNA Delivery System. *Nanoscale* **2011**, *3* (9), 3923−3932.

(9) Lin, J.-J.; Lin, W.-C.; Li, S.-D.; Lin, C.-Y.; Hsu, S.-h. Evaluation of the Antibacterial Activity and Biocompatibility for Silver Nanoparticles Immobilized on Nano Silicate Platelets. *ACS Appl. Mater. Interfaces* **2013**, *5* (2), 433−443.

(10) Qi, G.; Li., L.; Yu, F.; Wang, F. Vancomycin-Modified Mesoporous Silica Nanoparticles for Selective Recognition and Killing of Pathogenic Gram-Positive Bacteria Over Macrophage-Like Cells. *ACS Appl. Mater. Interfaces* **2013**, *5* (21), 10874−10881.

(11) Setyawati, M. I.; Fang, W.; Chia, S. L.; Leong, D. T. Nanotoxicology of Common Metal Oxide Based Nanomaterials: Their ROS-y and Non-ROS-y Consequences. *Asia-Pac. J. Chem. Eng.* **2013**, *8* (2), 205−217.

(12) Setyawati, M. I.; Khoo, P. K. S.; Eng, B. H.; Xiong, S.; Zhao, X.; Das, G. K.; Tan, T. T.-Y.; Loo, J. S. C.; Leong, D. T.; Ng, K. W. Cytotoxic and Genotoxic Characterization of Titanium Dioxide, Gadolinium Oxide, and Poly(Lactic-co-Glycolic Acid) Nanoparticles in Human Fibroblasts. *J. Biomed. Mater. Res., Part A* **2013**, *101A* (3), 633−640.

(13) Setyawati, M. I.; Tay, C. Y.; Chia, S. L.; Goh, S. L.; Fang, W.; Neo, M. J.; Chong, H. C.; Tan, S. M.; Loo, S. C.; Ng, K. W.; Xie, J. P.; Ong, C. N.; Tan, N. S.; Leong, D. T. Titanium Dioxide Nanomaterials Cause Endothelial Cell Leakiness by Disrupting the Homophilic Interaction of VE-cadherin. *Nat. Commun.* **2013**, *4*, 1673.

(14) Setyawati, M. I.; Tay, C. Y.; Leong, D. T. Effect of Zinc Oxide Nanomaterials-Induced Oxidative Stress on the p53 Pathway. *Biomaterials* **2013**, *34* (38), 10133−10142.

(15) Tay, C. Y.; Cai, P. Q.; Setyawati, M. I.; Fang, W.; Tan, L. P.; Hong, C. H. L.; Chen, X.; Leong, D. T. Nanoparticles Strengthen Intracellular Tension and Retard Cellular Migration. *Nano Lett.* **2014**, *14* (1), 83−88.

(16) Tay, C. Y.; Fang, W.; Setyawati, M. I.; Sum, C. P.; Xie, J.; Ng, K. W.; Chen, X.; Hong, C. H. L.; Leong, D. T. Reciprocal Response of Human Oral Epithelial Cells to Internalized Silica Nanoparticles. *Part. Part. Syst. Charact.* **2013**, *30* (9), 784−793.

(17) Tay, C. Y.; Fang, W.; Setyawati, M. I.; Chia, S. L.; Tan, K. S.; Hong, C. H. L.; Leong, D. T. Nano-hydroxyapatite and Nano-titanium Dioxide Exhibit Different Sub-cellular Distribution and Apoptotic Profile in Human Oral Epithelium. *ACS Appl. Mater. Interfaces* **2014**, *6* (9), 6248−6256.

(18) Li, J.; Pei, H.; Zhu, B.; Liang, L.; Wei, M.; He, Y.; Chen, N.; Li, D.; Huang, Q.; Fan, C. Self-Assembled Multivalent DNA Nanostructures for Noninvasive Intracellular Delivery of Immunostimulatory CpG Oligonucleotides. *ACS Nano* **2011**, *5* (11), 8783−8789.

(19) Kim, K. R.; Kim, D. R.; Lee, T.; Yhee, J. Y.; Kim, B. S.; Kwon, I. C.; Ahn, D. R. Drug Delivery by a Self-Assembled DNA Tetrahedron for Overcoming Drug Resistance in Breast Cancer Cells. *Chem. Commun.* **2013**, *49* (20), 2010−2012.

(20) Yuan, L.; Giovanni, M.; Xie, J.; Fan, C.; Leong, D. T. Ultrasensitive IgG Quantification Using DNA Nano-pyramids. *NPG Asia Mater.* **2014**, DOI: 10.1038/am.2014.46.

(21) Abi, A.; Lin, M.; Pei, H.; Fan, C.; Ferapontova, E. E.; Zuo, X. Electrochemical Switching with 3D DNA Tetrahedral Nanostructures

Self-Assembled at Gold Electrodes. *ACS Appl. Mater. Interfaces* **2014**, *6* (11), 8928−8931.

(22) Pei, H.; Lu, N.; Wen, Y.; Song, S.; Liu, Y.; Yan, H.; Fan, C. A DNA Nanostructure-Based Biomolecular Probe Carrier Platform for Electrochemical Biosensing. *Adv. Mater.* **2010**, *22* (42), 4754−4758.

(23) Bandy, T. J.; Brewer, A.; Burns, J. R.; Marth, G.; Nguyen, T.; Stulz, E. DNA as Supramolecular Scaffold for Functional Molecules: Progress in DNA Nanotechnology. *Chem. Soc. Rev.* **2011**, *40* (1), 138−148.

(24) Ke, Y.; Lindsay, S.; Chang, Y.; Liu, Y.; Yan, H. Self-assembled Water-soluble Nucleic Acid Probe Tiles for Label-free RNA Hybridization Assays. *Science* **2008**, *319* (5860), 180−183.

(25) Park, S. H.; Pistol, C.; Ahn, S. J.; Reif, J. H.; Lebeck, A. R.; Dwyer, C.; LaBean, T. H. Finite-size, Fully Addressable DNA Tile Lattices Formed by Hierarchical Assembly Procedures. *Angew. Chem., Int. Ed.* **2006**, *45* (5), 735−739.

(26) Mirkin, C. A. Programming the Assembly of Two- and Three-dimensional Architectures with DNA and Nanoscale Inorganic Building Blocks. *Inorg. Chem.* **2000**, *39* (11), 2258−2272.

(27) Clewell, D. B.; Evenchik, B. G. Effects of Rifampicin, Streptolydigin and Actinomycin D on the Replication of Col E1 Plasmid DNA in *Escherichia coli*. *J. Mol. Biol.* **1973**, *75* (3), 503−513.

(28) Krugh, T. R. Association of Actinomycin D and Deoxyribodinucleotides as a Model for Binding of the Drug to DNA. *Proc. Natl. Acad. Sci. U.S.A.* **1972**, *69* (7), 1911−1914.

(29) Weiss, J.; Beckerdite-Quagliata, S.; Elsbach, P. Resistance of Gram-negative Bacteria to Purified Bactericidal Leukocyte Proteins: Relation to Binding and Bacterial Lipopolysaccharide Structure. *J. Clin. Invest.* **1980**, *65* (3), 619−628.

(30) Crist, B. V. *Handbook of Monochromatic XPS Spectra*. Wiley: Chichester, U.K., 2000.

(31) Moulder, J. F; Stickle, W. F.; Sobol, P. E.; K.D, B. *Handbook of X-ray Photoelectron Spectroscopy*. Perkin-Elmer Corporation: Eden Prairie, MN, 1992.

(32) Manders, E. M. M.; Verbeek, F. J.; Aten, J. A. Measurement of Co-localization of Objects in Dual-Colour Confocal Images. *J. Microsc.* **1993**, *169*, 375−382.

(33) Dunn, K. W.; Kamocka, M. M.; McDonald, J. H. A Practical Guide to Eevaluating Colocalization in Biological Microscopy. *Am. J. Physiol.: Cell Physiol.* **2011**, *300* (4), C723−742.

(34) Yuan, X.; Luo, Z.; Zhang, Q.; Zhang, X.; Zheng, Y.; Lee, J. Y.; Xie, J. Synthesis of Highly Fluorescent Metal (Ag, Au, Pt, and Cu) Nanoclusters by Electrostatically Induced Reversible Phase Transfer. *ACS Nano* **2011**, *5* (11), 8800−8808.

(35) Luo, Z.; Yuan, X.; Yu, Y.; Zhang, Q.; Leong, D. T.; Lee, J. Y.; Xie, J. From Aggregation-Induced Emission of Au(I)-Thiolate Complexes to Ultrabright Au(0)@Au(I)-Thiolate Core-Shell Nanoclusters. *J. Am. Chem. Soc.* **2012**, *134* (40), 16662−16670.

(36) Yu, Y.; Luo, Z.; Chevrier, D. M.; Leong, D. T.; Zhang, P.; Jiang, D.-e.; Xie, J. Identification of a Highly Luminescent $Au_{22}(SG)_{18}$ Nanocluster. *J. Am. Chem. Soc.* **2014**, *136* (4), 1246−1249.

(37) Tay, C. Y.; Yu, Y.; Setyawati, M. I.; Xie, J.; Leong, D. T. Presentation Matters: Identity of Gold Nanoclusters Capping Agent Governs Intracellular Uptake and Cell Metabolism. *Nano Res.* **2014**, DOI: 10.1007/s12274-014-0441-z.

(38) Negishi, Y.; Nobusada, K.; Tsukuda, T. Glutathione-Protected Gold Clusters Revisited: Bridging the Gap Between Gold(I)-Thiolate Complexes and Thiolate-Protected Gold Nanocrystals. *J. Am. Chem. Soc.* **2005**, *127* (14), 5261−5270.

(39) Habeeb Muhammed, M. A.; Pradeep, T. Aqueous to Organic Phase Transfer of Au25 Clusters. *J. Cluster Sci.* **2009**, *20* (2), 365−373.

(40) Sobell, H. M.; Jain, S. C. Stereochemistry of Actinomycin Binding to DNA. II. Detailed Molecular Model of Actinomycin-DNA Complex and Its Implications. *J. Mol. Biol.* **1972**, *68* (1), 21−34.

(41) Einstein, A. The motion of elements suspended in static liquids as claimed in the molecular kinetic theory of heat. *Ann. Phys.* **1905**, *17* (8), 549−560.

(42) Lee, C.-Y.; Gong, P.; Harbers, G. M.; Grainger, D. W.; Castner, D. G.; Gamble, L. J. Surface Coverage and Structure of Mixed DNA/Alkylthiol Monolayers on Gold: Characterization by XPS, NEXAFS, and

Fluorescence Intensity Measurements. *Anal. Chem.* **2006**, *78* (10), 3316−3325.

(43) Castner, D. G.; Hinds, K.; Grainger, D. W. X-ray Photoelectron Spectroscopy Sulfur 2p Study of Organic Thiol and Disulfide Binding Interactions with Gold Surfaces. *Langmuir* **1996**, *12* (21), 5083−5086.

(44) Zhang, S.; Li, J.; Lykotrafitis, G.; Bao, G.; Suresh, S. Size-Dependent Endocytosis of Nanoparticles. *Adv. Mater.* **2009**, *21* (4), 419−424.

(45) Dubnau, D. DNA Uptake in Bacteria. *Annu. Rev. Microbiol.* **1999**, *53*, 217−244.

(46) Muschel, L. H.; Larsen, L. J. Actinomycin D Sensitivity of Bcteria with Simple and Complex Cell Surfaces. *J. Bacteriol.* **1969**, *98* (2), 840−841.

(47) Yuan, X.; Setyawati, M. I.; Leong, D. T.; Xie, J. Ultrasmall Ag^+-Rich Nanoclusters as Highly Efficient Nanoreservoirs for Bacterial Killing. *Nano Res.* **2014**, *7* (3), 301−307.

(48) Roth, B. L.; Poot, M.; Yue, S. T.; Millard, P. J. Bacterial Viability and Antibiotic Susceptibility Testing with SYTOX Green Nucleic Acid Stain. *Appl. Environ. Microbiol.* **1997**, *63* (6), 2421−2431.

(49) Wilks, J. C.; Slonczewski, J. L. pH of the Cytoplasm and Periplasm of *Escherichia coli*: Rapid Measurement by Green Fluorescent Protein Fluorimetry. *J. Bacteriol.* **2007**, *189* (15), 5601−5607.

(50) Marks, L. R.; Clementi, E. A.; Hakansson, A. P. Sensitization of *Staphylococcus aureus* to Methicillin and Other Antibiotics In Vitro and In Vivo in the Presence of HAMLET. *PLoS One* **2013**, *8* (5), e63158.

(51) Okabayaski, K.; Mizuno, D. Surface-Bound Nuclease of *Staphylococcus aureus*: Localization of the Enzyme. *J. Bacteriol.* **1974**, *117* (1), 215−221.

(52) Obinata, M.; Mizuno, D. Intracellular Localization of Deoxyribonucleases in *Escherichia coli*. *Biochim. Biophys. Acta* **1968**, *155* (1), 98−106.

(53) Shortman, K.; Lehman, I. R. The Deoxyribonucleases of *Escherichia coli*. VI. Changes in Enzyme Levels in Response to Alterations in Physiological State. *J. Biol. Chem.* **1964**, *239*, 2964−2974.

(54) Troller, J. A.; Stinson, J. V. Influence of Water Activity on the Production of Extracellular Enzymes by *Staphylococcus aureus*. *Appl. Environ. Microbiol.* **1978**, *35* (3), 521−526.

(55) Boone, D. L.; Tsang, B. K. Identification and Localization of Deoxyribonuclease I in the Rat Ovary. *Biol. Reprod.* **1997**, *57* (4), 813−821.

(56) Durphy, M.; Manley, P. N.; Friedberg, E. C. A Demonstration of Several Deoxyribonuclease Activities in Mammalian Cell Mitochondria. *J. Cell Biol.* **1974**, *62* (3), 695−706.